Pesq. Vet. Bras. 46:e07826, 2026
DOI: 10.1590/1678-5150-PVB-7826

Original Article
Small Animal Diseases

Mechanistic investigation of miR-144-3p in suppressing hepatocellular carcinoma progression via the NFE2L2/Nrf2 axis[1]

Chaoqun Liu[2], Boke Sun[2], Zhijun Guo[2], Derui Gou[2], Hongqiang Yao[2,3]*, Siriguleng Yu[2,3]

Chaoqun Liu – https://orcid.org/0009-0002-2220-6811
Boke Sun – https://orcid.org/0009-0008-2301-7100
Zhijun Guo – https://orcid.org/0009-0004-9821-4089
Derui Gou – https://orcid.org/0009-0001-8681-7470
Hongqiang Yao – https://orcid.org/0009-0008-7598-8953
Siriguleng Yu – https://orcid.org/0009-0002-3816-4724

ABSTRACT.- Liu CQ, Sun B, Guo ZJ, Gou DR, Yao HQ, Yu S. **Mechanistic investigation of miR-144-3p in suppressing hepatocellular carcinoma progression via the NFE2L2/Nrf2 axis.** *Pesquisa Veterinária Brasileira 46:e07826, 2026.* College of Veterinary Medicine, Inner Mongolia Agricultural University, Hohhot 010011, China. E-mail: yaohq66@126.com

Hepatocellular carcinoma (HCC) is a highly aggressive malignancy with frequent metastasis and limited therapeutic options. MicroRNAs are important regulators of tumor progression, but the role and downstream mechanism of miR-144-3p in HCC remain incompletely defined. In this study, we investigated the antitumor activity of miR-144-3p and its relationship with the NFE2L2/Nrf2 pathway. *In vitro*, miR-144-3p overexpression reduced Hep3B cell viability, inhibited cell-cycle progression, promoted apoptosis, and suppressed migration and invasion. Target prediction and dual-luciferase reporter assays supported NFE2L2, which encodes Nrf2, as a direct target of miR-144-3p. Consistently, miR-144-3p reduced Nrf2 expression and downregulated downstream Nrf2-related proteins, including NQO1 and HMOX1, with effects similar to Nrf2 knockdown. Reanalysis of a publicly available single-cell RNA sequencing dataset identified an Nfe2l2-positive hepatocyte progenitor cell subpopulation enriched in HCC and associated with invasion-, metastasis-, and stemness-related activity. *In vivo*, intratumoral administration of miR-144-3p agomir inhibited Hep3B-derived xenograft growth, increased apoptosis, and reduced Ki67 expression. These findings suggest that miR-144-3p suppresses HCC progression, at least in part, by targeting the NFE2L2/Nrf2 pathway, providing preliminary evidence of its biological relevance in comparative oncology and veterinary biomedical research.

INDEX TERMS: Hepatocellular carcinoma, miR-144-3p, NFE2L2/Nrf2 signaling, apoptosis.

INTRODUCTION

Hepatocellular carcinoma (HCC) is the most common primary liver malignancy and a leading cause of cancer-related mortality worldwide (Siegel et al. 2022). Despite advances in surgical resection, locoregional therapies, and systemic treatments, the prognosis of patients with advanced HCC remains poor due to high rates of recurrence, metastasis, and therapeutic resistance (Chidambaranathan-Reghupaty et al. 2021). The molecular heterogeneity of HCC poses a major challenge to effective treatment, underscoring the need to identify novel regulatory mechanisms and therapeutic targets involved in HCC initiation and progression.

MicroRNAs (miRNAs) are a class of small noncoding RNAs that regulate gene expression post-transcriptionally and play crucial roles in cancer-related processes, including cell proliferation, apoptosis, invasion, and stemness (Ratti et al. 2020). Dysregulation of miRNAs has been extensively implicated in HCC pathogenesis, with miRNAs functioning as oncogenes or tumor suppressors by modulating key signaling pathways (Lin et al. 2024). Among these, miR-144-3p has been reported to exert tumor-suppressive effects in

[1] Received on March 30, 2026.
Accepted for publication on June 12, 2026.
[2] College of Veterinary Medicine, Inner Mongolia Agricultural University, Inner Mongolia Autonomous Region, Hohhot, 010011, China. *Corresponding author: yaohq66@126.com
[3] Key Laboratory of Clinical Diagnosis and Treatment Technology for Animal Diseases, Ministry of Agriculture, Inner Mongolia Autonomous Region, Hohhot, 010011, China.

several malignancies (Lu et al. 2021); however, its delivery mode and key downstream targets in HCC remain incompletely understood.

Exosomes are nanosized extracellular vesicles that mediate intercellular communication by transferring bioactive cargo, including miRNAs, proteins, and lipids (McMasters et al. 2021). Due to their stability, biocompatibility, and ability to cross biological barriers, exosomes have emerged as promising vehicles for miRNA-based therapeutics (Chavda et al. 2023). Despite increasing evidence supporting the involvement of miRNAs in HCC progression, the functional role and downstream regulatory mechanism of miR-144-3p in HCC remain incompletely defined (Lin et al. 2024). In particular, whether miR-144-3p directly regulates NFE2L2/Nrf2 signaling and thereby affects malignant phenotypes of HCC cells requires further investigation.

In parallel, accumulating evidence indicates that HCC progression is driven by pronounced intratumoral heterogeneity, with progenitor-like cell populations contributing to tumor aggressiveness and metastasis (Aizarani et al. 2019, Chan et al. 2022). Single-cell RNA sequencing (scRNA-seq) has emerged as a powerful tool to dissect cellular heterogeneity and identify malignant subpopulations within tumors (Peng et al. 2019). Among oncogenic pathways implicated in HCC, the nuclear factor erythroid 2 – related factor 2 (Nrf2) signaling pathway plays a dual role in liver physiology and cancer (Gan et al. 2024). While transient Nrf2 activation protects hepatocytes against oxidative stress, sustained activation of Nrf2 promotes tumor cell survival, metabolic reprogramming, and resistance to therapy. However, the regulatory mechanisms controlling Nrf2 activation at the single-cell level in HCC remain poorly defined.

In this study, we investigated the miR-144-3p–NFE2L2/Nrf2 regulatory axis in HCC and provided new insights into the therapeutic potential of miR-144-3p-based targeting of Nrf2 signaling for liver cancer treatment.

MATERIALS AND METHODS

Ethical approval. This research protocol was reviewed and approved by the Laboratory Animal Welfare and Ethics Committee of Inner Mongolia Agricultural University (No. NND2024089) for ethical considerations, and all procedures were conducted in accordance with institutional guidelines for the care and use of laboratory animals.

Cell culture and transfection. The human hepatocellular carcinoma cell line Hep3B was obtained from Obio Technology (Shanghai, China). Cells were maintained in an incubator at 37 °C with 10% CO_2 and cultured in Dulbecco's Modified Eagle's Medium (DMEM) supplemented with 10% fetal bovine serum (FBS), 100 U/mL penicillin, and 100 μg/mL streptomycin. The miR-144-3p mimics and corresponding negative control (mimics NC), as well as small interfering RNA targeting Nrf2 (si-Nrf2) and its negative control (si-NC), were synthesized by Obio Technology (Shanghai, China). Prior to transfection, Hep3B cells were cultured to the logarithmic growth phase and adjusted to a density of 2×10^5 cells/mL. Subsequently, 1 mL of cell suspension was seeded into each well of the six-well plates. When appropriate confluence was reached, cells were transfected with miR-144-3p mimics or mimics NC, and si-Nrf2 or si-NC using Lipo8000™ transfection reagent (C0533, Beyotime, Shanghai, China). After 48 h of transfection, cells were harvested for subsequent experiments. All experimental procedures were performed in strict accordance with the manufacturers' protocols.

Cell viability assay. Cell viability was evaluated using the CCK-8 assay (C0037, Beyotime). Cells (5×10^4 cells/mL) were seeded into 96-well plates and cultured for 24, 48, and 72 h. CCK-8 solution (10 μL) was added to each well and incubated for 2 h at 37 °C, after which absorbance at 450 nm was measured using a microplate reader.

TUNEL staining. TUNEL assays were performed to evaluate apoptosis in paraffin-embedded tumor tissue sections using a TUNEL detection kit (12156792910, Roche, Basel, Switzerland) according to the manufacturer's instructions. Subsequently, the sections were developed with diaminobenzidine (DAB) solution (ZLI-9017, ZSGB-BIO, Beijing, China) and counterstained with hematoxylin (C200902, Baso, Zhuhai, China) for 10 min. Finally, apoptotic cells were visualized and quantified under a fluorescence microscope (DM2500, Leica, Wetzlar, Germany).

Flow cytometry analysis. Cell cycle distribution was analyzed using a Cell Cycle Detection Kit (E-CK-A351, Elabscience, Wuhan, China). Cells were fixed overnight in 70% ethanol at 4 °C, treated with RNase A (100 μg/mL), and stained with propidium iodide (PI, 50 μg/mL). After washing three times with pre-cooled phosphate-buffered saline (PBS), cell cycle profiles were acquired using a BD FACSVerse flow cytometer (BD Biosciences, NJ, USA). Cell apoptosis was assessed using an Annexin V-FITC/PI apoptosis detection kit (E-CK-A211, Elabscience, Wuhan, China). Hep3B cells were incubated with Annexin V-FITC and PI for 15 min in the dark, and apoptotic cells were quantified using a BD FACSVerse flow cytometer (BD Biosciences, NJ, USA).

Transwell assay. Cell migration and invasion assays were performed using Transwell chambers (3422, Corning, NY, USA), with Matrigel-coated inserts (353097, Corning, USA) used for invasion analysis. Briefly, 300 μL of cell suspension was added to the upper chamber, and 600 μL of medium containing 15% fetal bovine serum was added to the lower chamber. After incubation for 24 h at 37 °C, non-migrated or non-invaded cells were removed, and the remaining cells were fixed with 4% paraformaldehyde and stained with hematoxylin

(C0107, Beyotime, Shanghai, China). Cells were photographed and counted under an IX71 microscope (Olympus, Tokyo, Japan).

Luciferase reporter gene assay. The wild-type and mutant luciferase reporter plasmids containing the NFE2L2 3′ untranslated region (3′UTR), namely pMIR-REPORT-NFE2L2-3′UTR-WT (H30072) and pMIR-REPORT-NFE2L2-3′UTR-MUT (H30073), were constructed by Obio Technology (Shanghai, China). Human embryonic kidney 293T cells were obtained from the Cell Bank of the Chinese Academy of Sciences (Shanghai, China). The reporter plasmids were co-transfected with miR-144-3p mimics or negative control mimics into 293T cells using Lipofectamine 3000 (L3000015, Invitrogen, CA, USA). After 48 h of transfection, luciferase activity was measured using a dual-luciferase reporter gene assay according to the manufacturer's instructions.

Real-time quantitative PCR analysis. Total RNA was extracted from cells using TRIzol reagent (15596026CN, Invitrogen, Carlsbad/CA, USA), according to the manufacturers' instructions. Reverse transcription and real-time quantitative polymerase chain reaction (RT-qPCR) analyses were performed using an ABI 7500 Real-Time PCR System (Thermo Fisher Scientific, Waltham/MA, USA). Relative gene expression levels were calculated using the $2^{-\Delta\Delta CT}$ method. Primers for miR-144-3p, U6, and GAPDH were purchased from Sangon Biotech (Shanghai, China), and the primer sequences used in this study are listed in Table 1.

Western blot analysis. Total protein was extracted from cells using pre-cooled RIPA buffer supplemented with PMSF (P0013B, Beyotime, Shanghai, China). After centrifugation, proteins were separated by SDS-PAGE and transferred onto polyvinylidene difluoride (PVDF) membranes. The membranes were blocked with 5% non-fat milk for 2 h at room temperature and subsequently incubated overnight at 4 °C with primary antibodies against Nrf2 (1:1000), NQO1 (1:1000), HMOX1 (1:2000), and GAPDH (1:2000) (Abcam, Cambridge, UK). After washing, the membranes were incubated with horseradish peroxidase (HRP)-conjugated secondary antibodies (ZB2301, ZSGB-BIO, Beijing, China) for 2 h at room temperature. Protein bands were visualized using SuperSensitive ECL solution (ECL-0011, DingGuo ChangSheng Biotechnology, Beijing, China).

Single-cell RNA sequencing analysis of an external GEO dataset. Single-cell RNA sequencing (scRNA-seq) data from the GEO dataset GSE237823 (three hepatocellular carcinoma mouse samples and one normal control) were analyzed using Seurat (v4.1.0). Cells were filtered based on 200–5,000 detected genes, 500–15,000 unique molecular identifiers (UMIs), and < 5% mitochondrial gene expression. Data were normalized using NormalizeData, and the top 3,000 highly variable genes were identified using FindVariableFeatures (vst method). After scaling, principal component analysis (PCA) was performed, and the number of PCs was determined by ElbowPlot. Dimensionality reduction was conducted using UMAP (n.neighbors = 30, dims = 1:20). Batch effects were corrected using Harmony, and clustering was performed using FindNeighbors and FindClusters (resolution = 0.5). Cell types were annotated based on CellMarker 2.0, and differentially expressed genes were identified using FindAllMarkers (min.pct = 0.1, logfc.threshold = 0.25, $p < 0.05$). Trajectory analysis was performed using Monocle with the DDRTree algorithm.

Cell-derived xenograft model. Eighteen 5-week-old female BALB/c nude mice (body weight: 18.04 ± 1.55 g) were obtained from GemPharmatech (Jiangsu, China) and acclimatized for one week under standard laboratory conditions. Camel plasma samples were randomly collected from six healthy adult Bactrian camels at a camel farm located in Alxa League, Inner Mongolia Autonomous Region, China. All camels were clinically healthy at the time of blood collection. Plasma samples were processed under sterile conditions. Prior to tumor cell inoculation, mice were anesthetized with 1% pentobarbital sodium (50 mg/kg) via intraperitoneal injection. Adequate anesthesia was confirmed by the absence of pedal withdrawal reflex, and the duration of anesthesia was approximately 30~40 min, which was sufficient for the injection procedure. Hep3B cells (1 × 107 cells/mL, 200 μL) were subcutaneously injected into the right axillary region of each mouse. When tumor volume reached approximately 137 mm^3, mice were randomly assigned to three groups: Model, miR-144-3p agomir, and Agomir NC. Mice in the miR-144-3p agomir group received intratumoral injection of miR-144-3p agomir (1 nmol/mouse) four times per week, while the corresponding control groups received the appropriate vehicle or agomir negative control. Tumor volume and body weight were measured twice weekly, and tumor volume was calculated as 0.5 × length × $width^2$. *In vivo* bioluminescence was monitored with an IVIS Spectrum system (PerkinElmer, USA), and emitted signals were expressed as radiance (photons/sec/cm^2/sr). After 28 days, mice were euthanized by intraperitoneal administration of an overdose of 1% pentobarbital sodium (100 mg/kg), and tumor tissues were collected.

Immunohistochemistry. Paraffin-embedded sections were deparaffinized and rehydrated, followed by antigen retrieval. After blocking with goat serum for 1 h at room temperature, the sections were incubated overnight at 4 °C with an anti-Ki67 antibody (1:200, ab16667, Abcam, Cambridge, UK). The sections were then incubated with horseradish peroxidase (HRP)-conjugated goat anti-rabbit IgG (ZB2301, ZSGB-BIO, Beijing, China) for 1 h at room temperature, and immunoreactivity was visualized using diaminobenzidine. Ki67-positive cells were observed under an inverted microscope (IX71, Olympus, Tokyo, Japan), and the positive rate was calculated.

Statistical analysis. All quantitative data are presented as the mean ± standard deviation (SD). *In vitro* experiments were performed with at least three independent biological replicates unless otherwise stated.

Statistical analyses were performed using SPSS software version 21.0 (SPSS Inc., Chicago/IL, USA). Comparisons among multiple groups were conducted using one-way analysis of variance (ANOVA), followed by Tukey's post hoc test, while comparisons between two groups were performed using Student's t-test. For scRNA-seq analysis, adjusted *p*-values were used to correct for multiple comparisons in differential expression analysis. $p < 0.05$ or adjusted $p < 0.05$, where appropriate, was considered statistically significant.

RESULTS

miR-144-3p suppresses malignant phenotypes of Hep3B cells

To investigate the function of miR-144-3p in hepatocellular carcinoma, Hep3B cells were transfected with miR-144-3p mimics (Fig. 1). CCK-8 assays showed that miR-144-3p overexpression significantly reduced Hep3B cell viability compared with the mimics NC group (Fig. 2–3). Flow cytometric analysis revealed a decreased proportion of S-phase cells and increased apoptosis, predominantly early apoptosis, following miR-144-3p overexpression (Fig. 4–6). Transwell assays further demonstrated that cell migration and invasion were markedly inhibited in the mimics group (Fig. 7–10). Collectively, these results indicate that miR-144-3p suppresses Hep3B cell proliferation, cell-cycle progression, migration, and invasion, while promoting apoptosis.

miR-144-3p suppresses NFE2L2/Nrf2 signaling in Hep3B cells

To explore the molecular mechanism of miR-144-3p in hepatocellular carcinoma (HCC), potential target mRNAs were predicted using the StarBase database[4], identifying NFE2L2 (encoding Nrf2) as a candidate target of miR-144-3p (Fig. 11). Dual-luciferase reporter assays revealed that miR-144-3p significantly reduced luciferase activity of the wild-type NFE2L2 3′UTR reporter, but not the mutant construct, confirming a direct interaction between miR-144-3p and NFE2L2 (Fig. 12). Consistent with these findings, overexpression of miR-144-3p in Hep3B cells led to a significant decrease in Nrf2 mRNA expression (Fig. 13). NADPH quinone oxidoreductase 1 (NQO1) and heme oxygenase 1 (HMOX1) are target genes of Nrf2, and Nrf2 promotes tumor cell proliferation and invasion by promoting NQO1 and HMOX1 expression (Li et al. 2022). Western blot analysis confirmed that miR-144-3p overexpression significantly reduced the protein levels of Nrf2, NQO1, and HMOX1, with GAPDH used as the loading control (Fig. 14). Additionally, the protein expression of Nrf2, NQO1, and HMOX1 was quantified in Hep3B cells under different treatments: control, miR-144-3p mimics, mimics-NC, si-Nrf2, and si-NC. The results showed that overexpression of miR-144-3p significantly decreased the expression of Nrf2, NQO1, and HMOX1 compared to the control, with effects similar to those observed with Nrf2 knockdown using siRNA (Fig. 15–17).

Single-cell transcriptomic profiling identifies an Nfe2l2$^+$ malignant HPC subpopulation in HCC

To elucidate the cellular mechanisms underlying hepatocellular carcinoma (HCC) development and metastasis, single-cell RNA sequencing (scRNA-seq) was performed on HCC and control mouse liver samples. After quality control, highly variable gene selection, and principal component analysis, 27 cell clusters were identified (Fig. 18). UMAP visualization revealed a more heterogeneous cellular composition in HCC samples compared with controls (Fig. 19). Cell annotation defined 10 major cell types, including B cells, cholangiocytes, dendritic cells, endothelial cells, fibroblasts, hepatocytes/progenitor cells (HPCs), Kupffer cells, monocytes, NK cells, and T cells (Fig. 20–21). Notably, the proportion of HPCs was significantly increased in HCC samples (Fig. 22). Given this enrichment, HPCs were extracted for further analysis, yielding 16 subclusters (Fig. 23). UMAP analysis showed greater cellular diversity within HPCs from HCC samples than controls (Fig. 24). Based on marker gene expression, HPCs were classified into three subsets: Nfe2l2$^+$HPC, Saa1$^+$HPC and Selenbp2$^+$HPC (Fig. 25–26). Cell composition analysis demonstrated that Selenbp2$^+$HPCs predominated in control samples, whereas Nfe2l2$^+$HPCs were specifically enriched in HCC (Fig. 27). Functional scoring using CancerSEA gene sets and the UCELL algorithm revealed that Nfe2l2$^+$HPCs exhibited higher invasion, metastasis, and stemness scores (Fig. 28). Pseudotime trajectory analysis, with Selenbp2$^+$HPCs as the origin, showed a progressive upregulation of Nfe2l2 during HCC development (Fig. 29). Collectively, these findings indicate that Nfe2l2 upregulation marks a malignant HPC subpopulation and may drive HCC progression.

miR-144-3p agomir suppresses tumor growth and proliferation *in vivo*

To validate the *in vitro* findings, a Hep3B cell-derived xenograft (CDX) model was established in nude mice. When tumors reached approximately 137 mm^3, mice received intratumoral administration of miR-144-3p agomir or agomir negative control (Agomir NC), while untreated tumor-bearing mice served as the Model group. *In vivo* bioluminescence imaging revealed that mice treated with miR-144-3p agomir exhibited markedly reduced radiance in the tumor region compared with the Model and Agomir NC groups (Fig. 30). Consistently, tumor growth curves demonstrated significantly slower tumor progression in the miR-144-3p agomir group throughout the observation period (Fig. 31). At the experimental endpoint, tumors from the miR-144-3p agomir–

[4] https://rnasysu.com/encori/

treated mice were visibly smaller and displayed significantly lower tumor weights than those from the Model and Agomir NC groups (Fig. 32–33). TUNEL staining showed enhanced apoptosis in tumors from the miR-144-3p agomir group compared with controls (Fig. 34). In parallel, Ki67 immunohistochemistry revealed a pronounced decrease in proliferating cells following miR-144-3p agomir treatment (Fig. 35). Collectively, these results demonstrate that miR-144-3p agomir effectively suppresses HCC tumor growth *in vivo* by inhibiting tumor cell proliferation and promoting apoptosis.

DISCUSSION

In this study, we systematically investigated the antitumor role and underlying mechanism of miR-144-3p in hepatocellular carcinoma (HCC) by integrating *in vitro* functional assays, single-cell transcriptomic analysis, mechanistic validation, and *in vivo* xenograft models. Our findings suggest that miR-144-3p may exert tumor-suppressive effects in HCC by inhibiting malignant cell behaviors and suppressing the NFE2L2/Nrf2-associated redox signaling pathway. Integration with single-cell transcriptomic analysis further suggests the relevance of NFE2L2 in tumor cellular heterogeneity.

HCC remains one of the most prevalent and lethal malignancies worldwide, particularly in China, where late diagnosis and high rates of metastasis severely limit the effectiveness of curative treatments (Sung et al. 2021). The lack of early diagnostic biomarkers and the pronounced molecular heterogeneity of HCC underscore the urgent need for novel regulatory insights and therapeutic strategies. In this context, microRNA-based therapies have gained considerable attention (Sadeghi et al. 2023); however, their clinical application is largely constrained by the absence of safe and efficient delivery systems.

MiRNA-based therapeutic strategies have gained increasing attention because miRNAs can coordinately regulate multiple cancer-related pathways (Ratti et al. 2020). Previous studies have shown that animal plasma-derived exosomes are enriched with miR-144-3p, which may provide a potential basis for cross-species therapeutic applications (Chen et al. 2024). The present study provides experimental evidence that miR-144-3p exerts antitumor activity by inducing apoptosis and inhibiting malignant progression in HCC cells. Although human HCC cells were used as the main *in vitro* model, the relevance of this study to veterinary biomedical research lies in the evaluation of conserved miRNA-mediated regulatory mechanisms in mammalian tumor models.

Functionally, we showed that miR-144-3p suppressed HCC cell proliferation, cell cycle progression, migration, and invasion, while promoting apoptosis in Hep3B cells. These findings are consistent with previous reports describing the tumor-suppressive role of miR-144-3p in other malignancies (Li et al. 2021) and extend its relevance by demonstrating its inhibitory effects in an HCC model.

By reanalyzing a publicly available single-cell RNA sequencing dataset (GSE237823), we identified a distinct Nfe2l2^{+} hepatocyte progenitor cell (HPC) subpopulation selectively enriched in HCC tissues. Functional enrichment scoring suggested that this subpopulation exhibited higher stemness, invasion, and metastasis-related activity. These findings provide descriptive cellular context suggesting the potential relevance of Nfe2l2-positive hepatocyte progenitor cells in HCC progression, but further orthogonal validation is required.

Mechanistically, our dual-luciferase reporter assay supported a direct interaction between miR-144-3p and the NFE2L2 3′UTR. In addition, miR-144-3p overexpression reduced Nrf2 expression and decreased the levels of downstream Nrf2-related proteins, including NQO1 and HMOX1. The phenotypic similarity between miR-144-3p overexpression and siRNA-mediated Nrf2 knockdown further suggests that the NFE2L2/Nrf2 pathway may participate in the tumor-suppressive effects of miR-144-3p. While transient Nrf2 activation is protective in normal hepatocytes, sustained Nrf2 signaling in cancer cells supports redox homeostasis, survival, and therapeutic resistance. By inhibiting this pathway, miR-144-3p may disrupt Nrf2-dependent survival and proliferative programs in HCC cells. The antitumor efficacy of miR-144-3p was further validated *in vivo*. In a Hep3B-derived subcutaneous xenograft model, intratumoral administration of miR-144-3p agomir significantly reduced tumor growth, inhibited proliferation, and increased apoptosis, indicating its antitumor activity under this experimental setting.

Several limitations should be acknowledged. Rescue experiments using miR-144-3p-resistant Nrf2 overexpression were not performed, and the causal role of the NFE2L2/Nrf2 pathway requires further confirmation. In addition, the scRNA-seq analysis was based on a limited public dataset and remains descriptive, requiring orthogonal validation. The *in vivo* study was limited to a subcutaneous xenograft model in immunodeficient nude mice with intratumoral agomir administration; systemic delivery, toxicity, biodistribution, and orthotopic or immunocompetent models were not assessed. Finally, because human HCC cells and murine xenografts were used, the present findings provide only preliminary evidence for cross-species biological relevance, and further validation is needed to determine whether this regulatory mechanism is broadly applicable across animal species.

CONCLUSION

This study reveals a previously unrecognized miR-144-3p–NFE2L2/Nrf2 regulatory axis in HCC and links this axis to the malignant Nfe2l2+ HPC subpopulation. By integrating single-cell, mechanistic, and *in vivo* evidence, our findings advance the understanding of the miR-144-3p–NFE2L2/Nrf2 regulatory axis in tumor progression and provide preliminary experimental support for the biological potential of miR-144-3p in comparative biomedical research.

Funding.- This study was supported by the Natural Science Foundation of Inner Mongolia Autonomous Region (no. 2023MS03021 and 2024MS03071), and Municipal Major Special Program for Innovation Guidance in Science and Technology, China (No. K2024005).

Conflict of interest statement.- The authors declare that they have no conflict of interest.

Credit author statement.- Hongqiang Yao, Chaoqun Liu, Siriguleng Yu: Conception and design, obtaining funding, writing the article. Chaoqun Liu, Boke Sun, Zhijun Guo, Derui Gou: Writing the article, data collection, analysis and interpretation. Chaoqun Liu, Derui Gou: Methodology, formal analysis, writing the article.

Data availability statement.- The data supporting this study are available and can be accessed upon request from the corresponding author.

Editor-in-Chief.- Fabiano José Ferreira de Sant'Ana.

REFERENCES

Aizarani N, Saviano A, Sagar, Mailly L, Durand S, Herman JS, Pessaux P, Baumert TF, Grün D. A human liver cell atlas reveals heterogeneity and epithelial progenitors. Nature 2019; https://doi.org/10.1038/s41586-019-1373-2

Behrouz S, Saadat S, Memarzia A, Sarir H, Folkerts G, Boskabady MH. The Antioxidant, Anti-Inflammatory and Immunomodulatory Effects of Camel Milk. Front Immunol 2022; https://doi.org/10.3389/fimmu.2022.855342

Chan L-K, Tsui Y-M, Ho DW-H, Ng IO-L. Cellular heterogeneity and plasticity in liver cancer. Semin Cancer Biol 2022; https://doi.org/10.1016/j.semcancer.2021.02.015

Chavda VP, Pandya A, Kumar L, Raval N, Vora LK, Pulakkat S, Patravale V, Salwa, Duo Y, Tang BZ. Exosome nanovesicles: A potential carrier for therapeutic delivery. Nano Today 2023; https://doi.org/10.1016/j.nantod.2023.101771

Chen X, Luo Y, Zhu Q, Zhang J, Huang H, Kan Y, Li D, Xu M, Liu S, Li J, Pan J, Zhang L, Guo Y, Wang B, Qi G, Zhou Z, Zhang C-Y, Fang L, Wang Y, Chen X. Small extracellular vesicles from young plasma reverse age-related functional declines by improving mitochondrial energy metabolism. Nat Aging 2024; https://doi.org/10.1038/s43587-024-00612-4

Chidambaranathan-Reghupaty S, Fisher PB, Sarkar D. Hepatocellular carcinoma (HCC): epidemiology, etiology and molecular classification. In: Tew KD, Fisher PB. Advances in Cancer Research. 2021; https://doi.org/10.1016/bs.acr.2020.10.001

Gan L, Wang W, Jiang J, Tian K, Liu W, Cao Z. Dual role of Nrf2 signaling in hepatocellular carcinoma: promoting development, immune evasion, and therapeutic challenges. Front Immunol 2024; https://doi.org/10.3389/fimmu.2024.1429836

Khan MZ, Xiao J, Ma Y, Ma J, Liu S, Khan A, Khan JM, Cao Z. Research development on anti-microbial and antioxidant properties of camel milk and its role as an anti-cancer and anti-hepatitis agent. Antioxidants 2021; https://doi.org/10.3390/antiox10050788

Li S, Zhang Y, Zhang J, Yu B, Wang W, Jia B, Chang J, Liu J. Neferine exerts ferroptosis-inducing effect and antitumor effect on thyroid cancer through Nrf2/HO-1/NQO1 inhibition. J Oncol 2022; https://doi.org/10.1155/2022/7933775

Li T, Tang C, Huang Z, Yang L, Dai H, Tang B, Xiao B, Li J, Lei X. miR-144-3p inhibited the growth, metastasis and epithelial-mesenchymal transition of colorectal adenocarcinoma by targeting ZEB1/2. Aging 2021; https://doi.org/10.18632/aging.203225

Lin HT, Castaneda AFA, Krishna SG, Mumtaz K. MicroRNAs in hepatocellular carcinoma treatment: Charting the path forward. World J Gastroenterol 2024; https://doi.org/10.3748/wjg.v30.i11.1470

Lu Y, Zhang B, Wang B, Wu D, Wang C, Gao Y, Liang W, Xi H, Wang X, Chen L. MiR-144-3p inhibits gastric cancer progression and stemness via directly targeting GLI2 involved in hedgehog pathway. J Transl Med 2021; https://doi.org/10.1186/s12967-021-03093-w

McMasters A, McMasters KM, Hao H. Exosome to Promote Cancer Progression via Its Bioactive Cargoes. Cancer Biol 2021; https://doi.org/10.33696/cancerbiology.2.021

Peng J, Sun B-F, Chen C-Y, Zhou J-Y, Chen Y-S, Chen H, Liu L, Huang D, Jiang J, Cui G-S, Yang Y, Wang W, Guo D, Dai M, Guo J, Zhang T, Liao Q, Liu Y, Zhao Y-L, Han D-L, Zhao Y, Yang Y-G, Wu W. Single-cell RNA-seq highlights intra-tumoral heterogeneity and malignant progression in pancreatic ductal adenocarcinoma. Cell Res 2019; https://doi.org/10.1038/s41422-019-0195-y

Ratti M, Lampis A, Ghidini M, Salati M, Mirchev MB, Valeri N, Hahne JC. MicroRNAs (miRNAs) and long non-coding RNAs (lncRNAs) as new tools for cancer therapy: first steps from bench to bedside. Target Oncol 2020; https://doi.org/10.1007/s11523-020-00717-x

Sadeghi S, Tehrani FR, Tahmasebi S, Shafiee A, Hashemi SM. Exosome engineering in cell therapy and drug delivery. Inflammopharmacology 2023; https://doi.org/10.1007/s10787-022-01115-7

Samarpita S, Li X. Leveraging exosomes as the next-generation bio-shuttles: the next biggest approach against Th17 cell catastrophe. Int J Mol Sci 2023; https://doi.org/10.3390/ijms24087647

Siegel RL, Miller KD, Fuchs HE, Jemal A. Cancer Statistics, 2022. CA Cancer J Clin 2022; https://doi.org/10.3322/caac.21708

Sung H, Ferlay J, Siegel RL, Laversanne M, Soerjomataram I, Jemal A, Bray F. Global Cancer Statistics 2020: GLOBOCAN estimates of incidence and mortality worldwide for 36 cancers in 185 countries. CA Cancer J Clin 2021; https://doi.org/10.3322/caac.21660

Figures

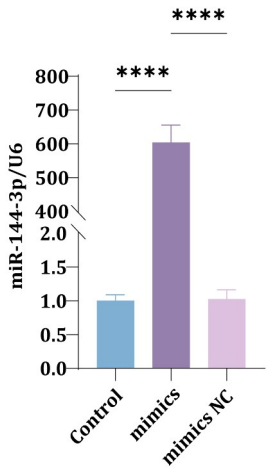
****
****
miR-144-3p/U6
800
700
600
500
400
2.0
1.5
1.0
0.5
0.0
Control
mimics
mimics NC

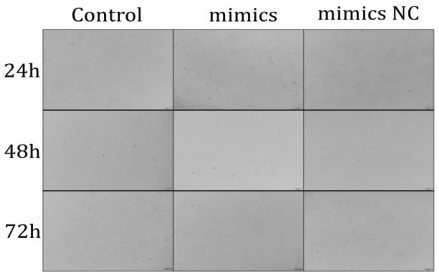
Control
mimics
mimics NC
24h
48h
72h

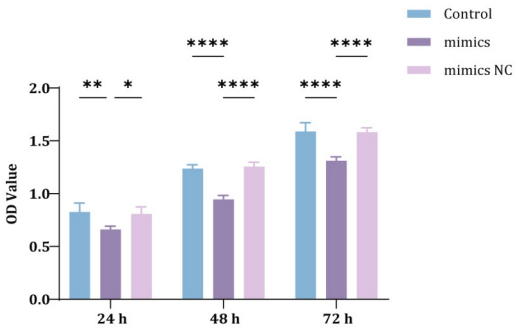
Control
mimics
mimics NC
**
*
****
****
****
OD Value
2.0
1.5
1.0
0.5
0.0
24 h
48 h
72 h

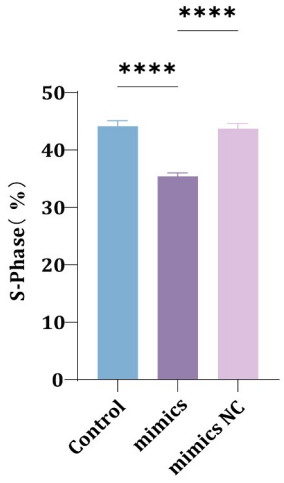
****
****
S-Phase（%）
50
40
30
20
10
0
Control
mimics
mimics NC

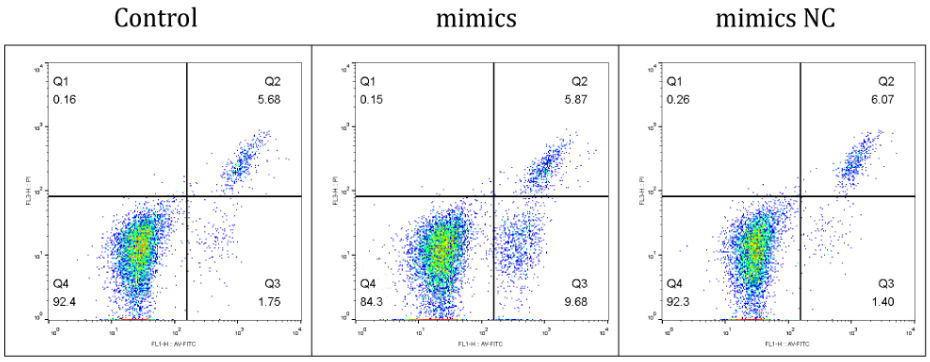
Control
mimics
mimics NC
Q1
0.16
Q2
5.68
Q4
92.4
Q3
1.75
Q1
0.15
Q2
5.87
Q4
84.3
Q3
9.68
Q1
0.26
Q2
6.07
Q4
92.3
Q3
1.40

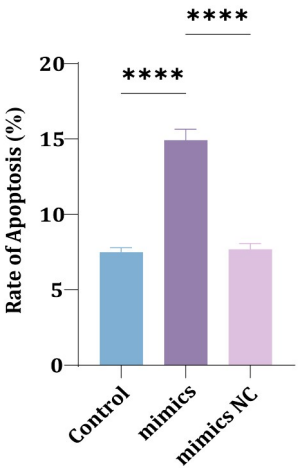
****
****
Rate of Apoptosis (%)
20
15
10
5
0
Control
mimics
mimics NC

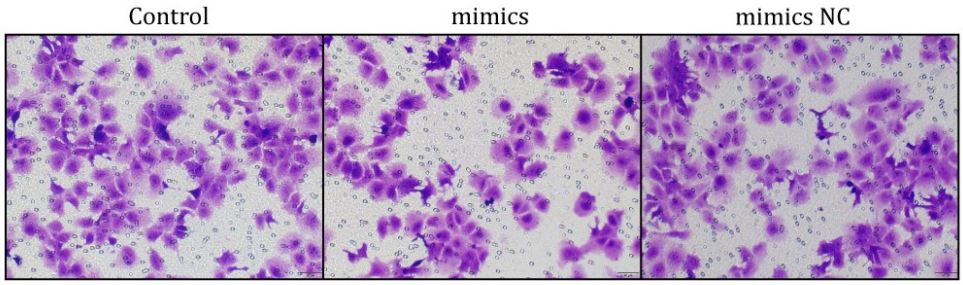
Control
mimics
mimics NC

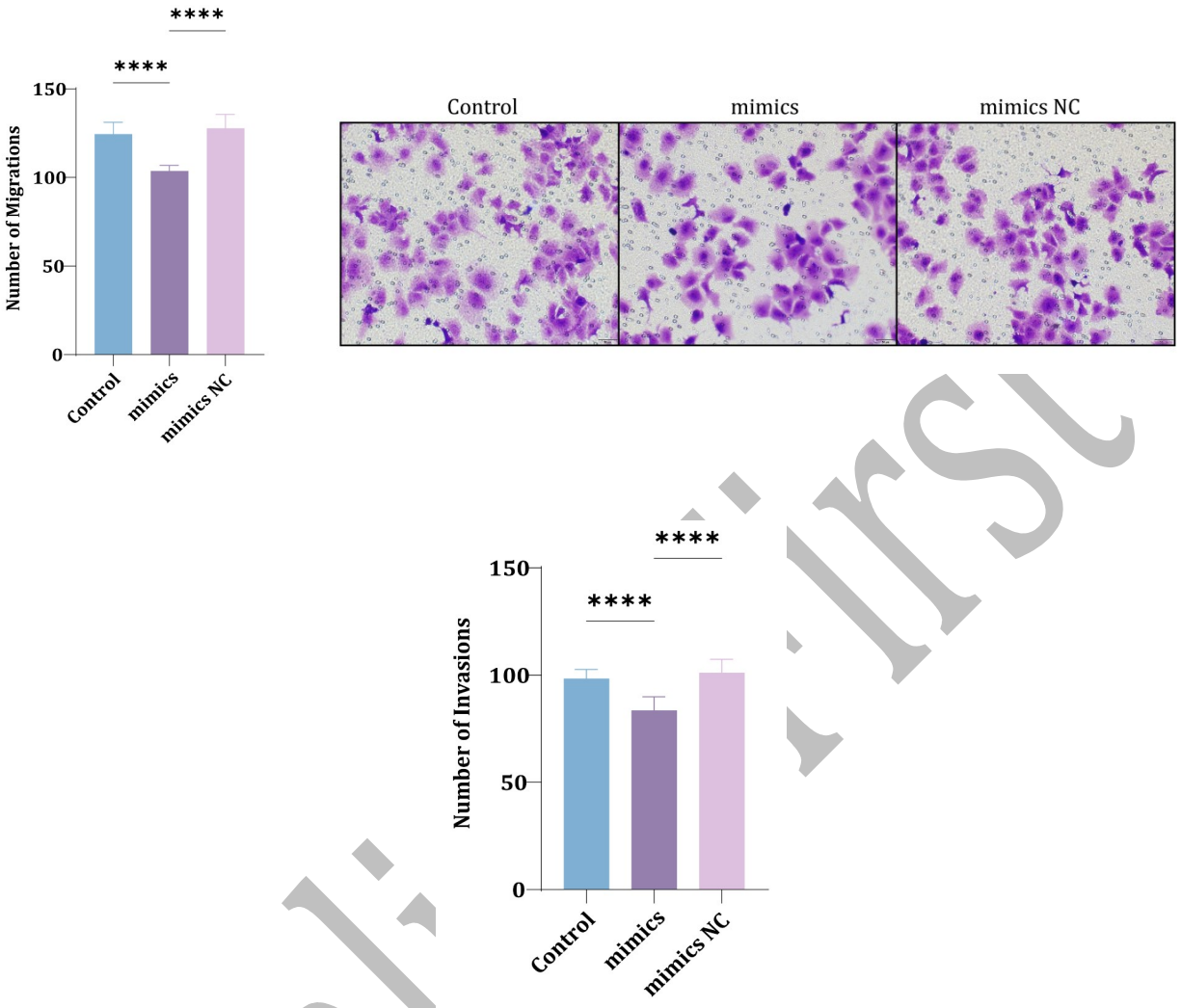

Fig. 1–10. miR-144-3p suppresses malignant phenotypes of Hep3B cells. (**1**) Transfection efficiency of miR-144-3p mimics in Hep3B cells. (**2**–**3**) CCK-8 assay showing that miR-144-3p overexpression significantly reduced cell viability compared with the mimics-negative control (NC). (**4**–**6**) Flow cytometric analyses indicate that miR-144-3p overexpression decreased the proportion of S-phase cells and increased apoptosis, primarily early apoptosis. (**7**–**10**) Transwell migration and invasion assays demonstrating that miR-144-3p overexpression markedly inhibited Hep3B cell motility and invasive capacity. Collectively, these data suggest that miR-144-3p inhibits Hep3B cell proliferation, cell-cycle progression, migration, and invasion while promoting apoptosis. *$p < 0.05$, **$p < 0.01$, ***$p < 0.001$, ****$p < 0.0001$ compared to control or NC.

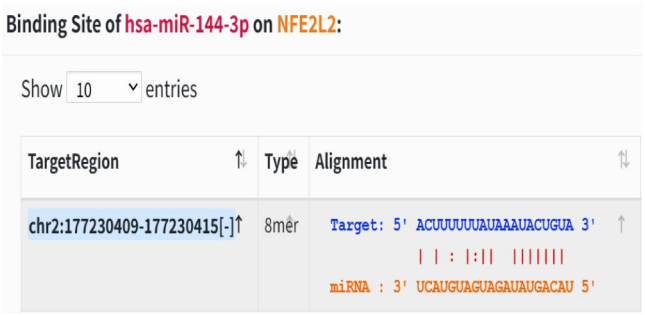

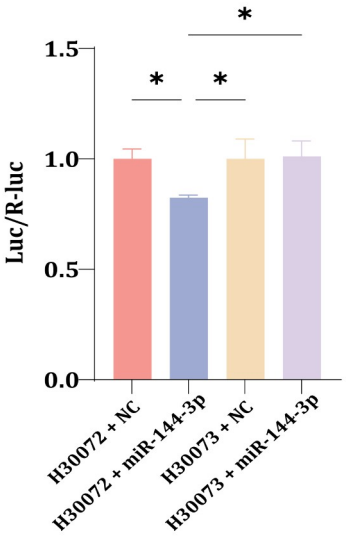
*
*
*
1.5
1.0
0.5
0.0
Luc/R-luc
H30072 + NC
H30072 + miR-144-3p
H30073 + NC
H30073 + miR-144-3p

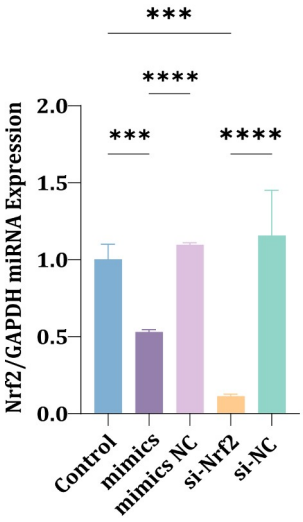
***
****
***
****
2.0
1.5
1.0
0.5
0.0
Nrf2/GAPDH miRNA Expression
Control
mimics
mimics NC
si-Nrf2
si-NC

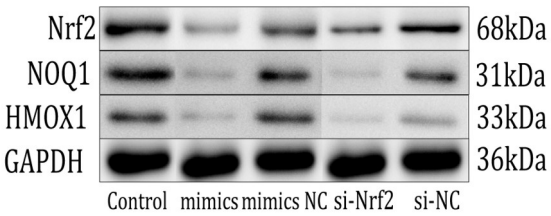
Nrf2
NOQ1
HMOX1
GAPDH
68kDa
31kDa
33kDa
36kDa
Control
mimics
mimics NC
si-Nrf2
si-NC

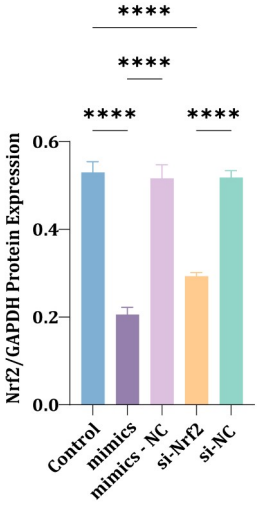

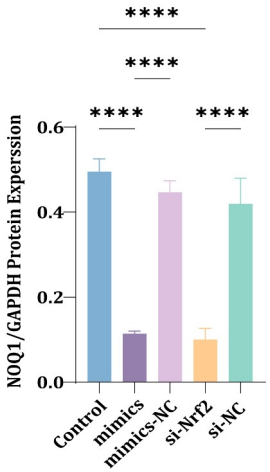

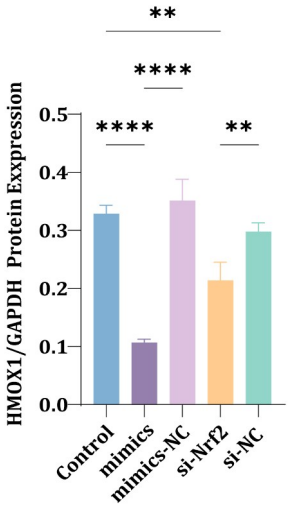

Fig. 11–17. miR-144-3p inhibits Nrf2-related gene and protein expression in Hep3B cells. (**11**) Binding site of hsa-miR-144-3p on NFE2L2 (Nrf2) predicted by bioinformatics analysis. (**12**) Luciferase reporter assay showing the effect of miR-144-3p on luciferase activity in Hep3B cells. *$p < 0.05$ compared to the control group. (**13**) Quantitative PCR analysis of Nrf2 mRNA expression in Hep3B cells transfected with miR-144-3p mimics, mimics-negative control (NC), si-Nrf2, and si-NC. (**14**) Western blot analysis of Nrf2, NOQ1, and HMOX1 protein

expression in Hep3B cells after transfection with miR-144-3p mimics, mimics-NC, si-Nrf2, and si-NC. GAPDH was used as a loading control. (**15**–**17**) Quantification of NOQ1/GAPDH protein expression. *$p < 0.05$, **$p < 0.01$, ***$p < 0.001$, ****$p < 0.0001$ compared to control or NC.

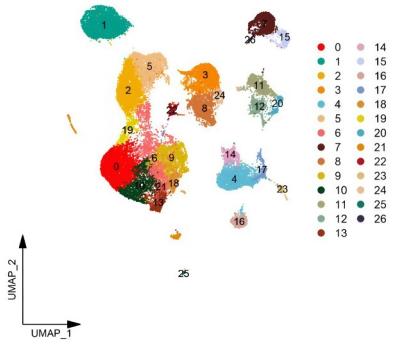

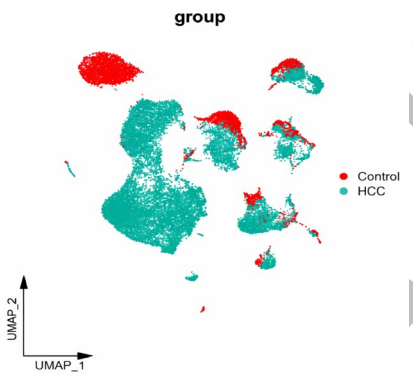

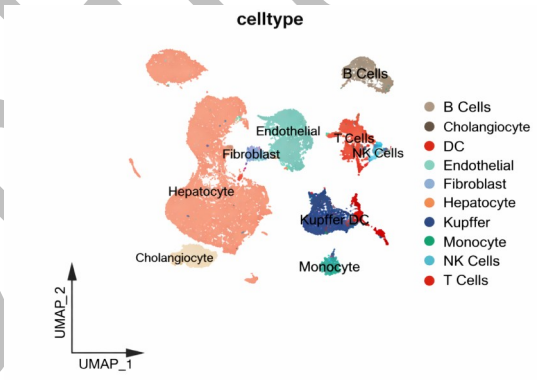

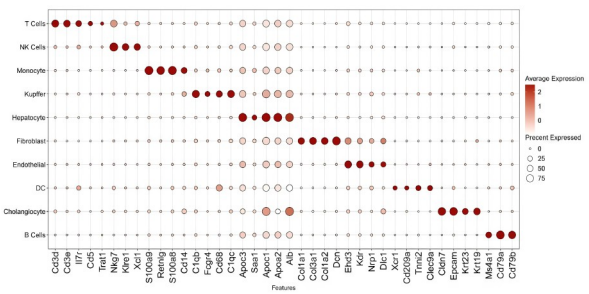

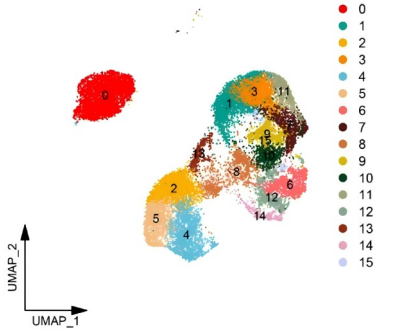

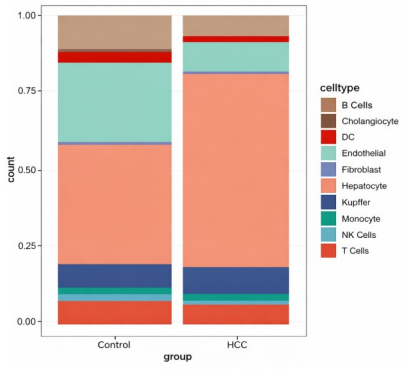

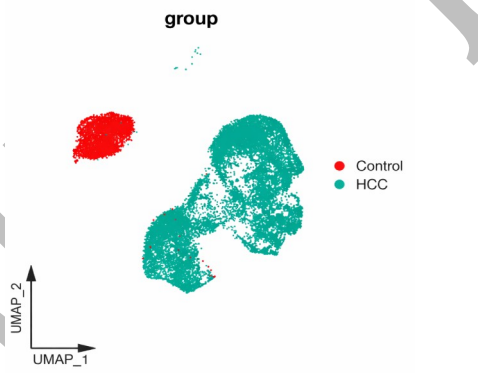

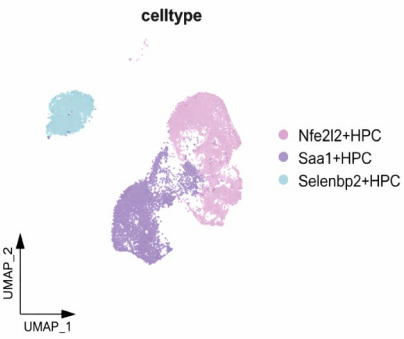

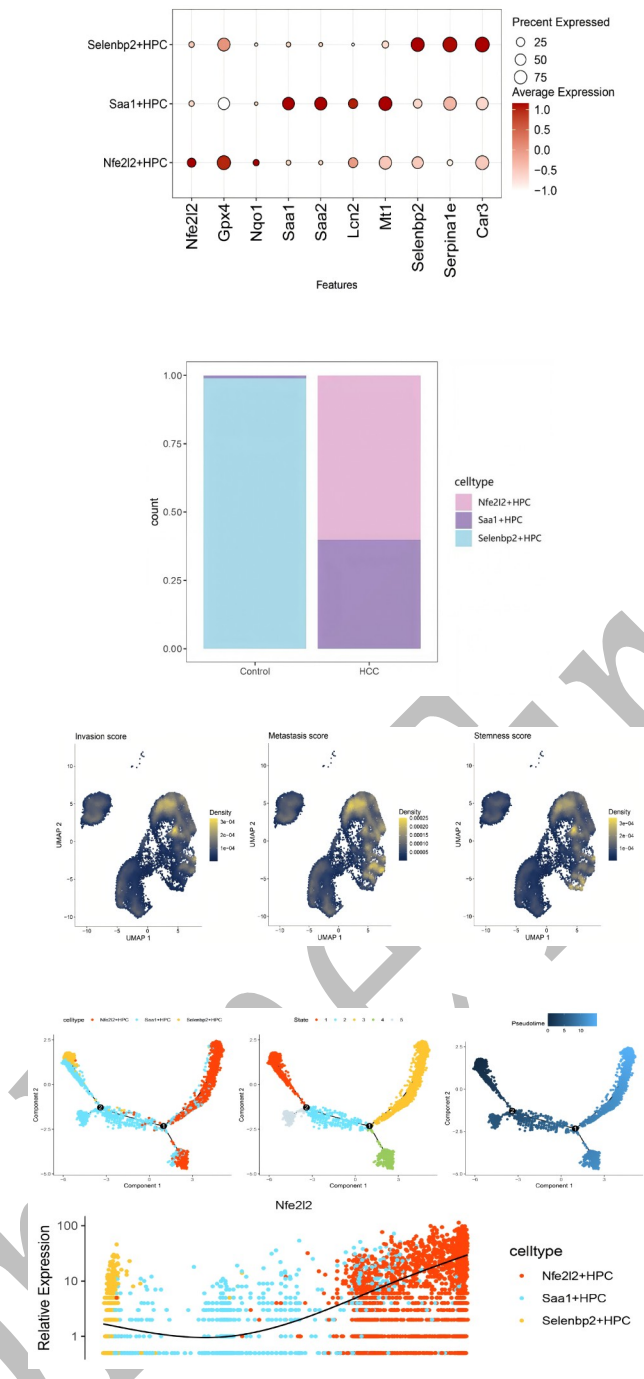

Fig. 18–29. .scRNA-seq analysis revealed the involvement of NFE2L2 in HCC development. (**18**) Plot of cell clusters. (**19**) UMAP plot of cellular distribution in different samples. (**20**) Cellular annotation results. (**21**) Bubble plots of markers used for cellular annotations. (**22**) Stacked histogram of cellular subsets in different samples. (**23**) Cellular subset map of HPCs. (**24**) UMAP plot of cell distribution in different samples. (**25**) Distribution of Nfe2l2+HPC, Saa1+HPC, Selenbp2+HPC. (**26**) Bubble plot of markers used for cellular annotations of Nfe2l2+HPC, Saa1+HPC, Selenbp2+HPC. (**27**) Stacked histogram of cell occupancy in different samples. (**28**) Highlighted plots of cell invasion, metastasis, and stemness scores. (**29**) Trajectory analysis results.

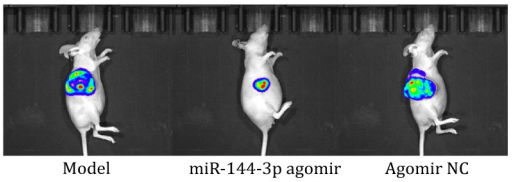

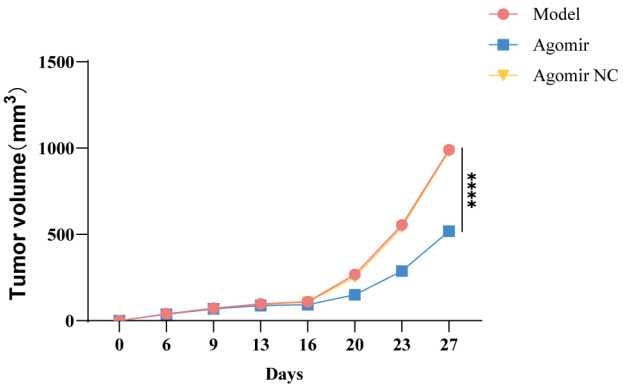
Model
Agomir
Agomir NC
Tumor volume(mm3)
1500
1000
500
0
0
6
9
13
16
20
23
27
Days
****

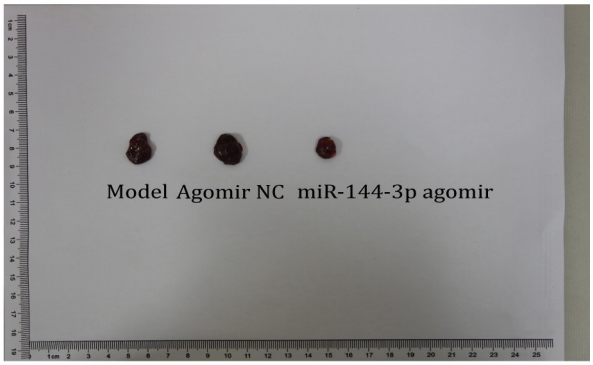
Model Agomir NC miR-144-3p agomir

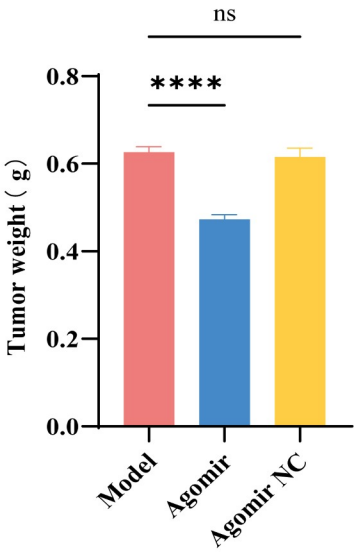
ns
****
Tumor weight (g)
0.8
0.6
0.4
0.2
0.0
Model
Agomir
Agomir NC

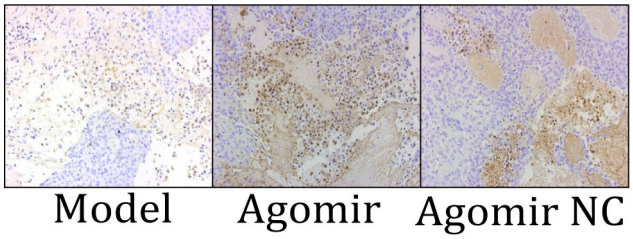
Model
Agomir
Agomir NC

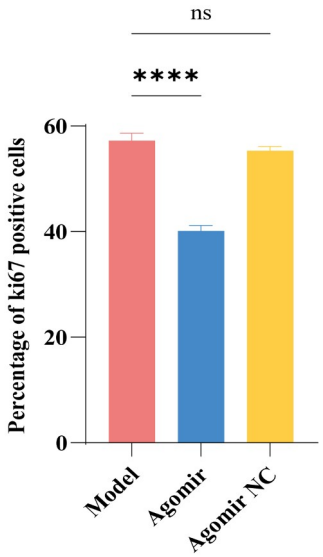

Fig. 30–35. miR-144-3p agomir suppresses HCC tumor growth *in vivo*. (**30**) Representative bioluminescence images of Hep3B-derived xenograft tumors in nude mice from the Model, miR-144-3p agomir, and Agomir negative control (NC) groups. Reduced luminescent signals indicate decreased tumor burden in the miR-144-3p agomir–treated group. (**31**) Tumor growth curves of each group were measured over the indicated time points. (**32**) Representative images of excised tumors at the experimental endpoint. (**33**) Quantification of tumor weights from each group. (**34**) Representative TUNEL staining of tumor sections showing apoptotic cells in each group. (**35**) Quantitative analysis of Ki67-positive cells based on immunohistochemical staining. **** $p < 0.0001$ compared to model or NC.

Table 1. Primer information in this study

Name	Forward primer (5'-3')	Reverse primer (5'-3')
miR-144-3p	GCGCGCGTACAGTATAGATGA	AGTGCAGGGTCCGAGGTATT
Nrf2	AGACAAACATTCAAGCCGCT	CCCCTCCTACGTATATCCCG
U6	CTCGCTTCGGCAGCACATATACT	ACGCTTCACGAATTTGCGTGTC
GAPDH	GGAGCGAGATCCCTCCAAAAT	GGCTGTTGTCATACTTCTCATGG